Reactive High Power Impulse Magnetron Sputtering Ti-Al-N coatings: film/substrate interface design effect on high temperature cyclic oxidation behavior.

S.M. Deambrosis*, F. Montagner*, V. Zin*, M. Fabrizio*, C. Badini**, E. Padovano**, M. Sebastiani^, E. Bemporad^, K. Brunelli[§&], E. Miorin*.

* National Research Council (CNR) of Italy, Institute of Condensed Matter Chemistry and Technologies for Energy (ICMATE)

Corso Stati Uniti 4 - 35127 Padova, Italy

** Politecnico di Torino, Department of Applied Science and Technology

C.so Duca degli Abruzzi 24 – 10129 Torino, Italy

^ University "Roma Tre", Engineering Department,

Via della Vasca Navale 79 - 00146 Rome, Italy

[§] University of Padova, Industrial Engineering Department,

Via Marzolo 9, 35131 Padova, Italy

[&] University of Padova, Department of Civil, Environmental and Architectural Engineering,

Via Marzolo 9, 35131 Padova, Italy

E-mails

silviamaria.deambrosis@cnr.it; francesco.montagner@cnr.it; valentina.zin@cnr.it; monica.fabrizio@cnr.it; claudio.badini@polito.it; elisa.padovano@polito.it; marco.sebastiani@uniroma3.it; edoardo.bemporad@uniroma3.it; katya.brunelli@unipd.it; enrico.miorin@cnr.it.

Corresponding Author

Name: Enrico

Surname: Miorin

Affiliation: National Research Council (CNR) of Italy, Institute of Condensed Matter Chemistry and Technologies for Energy (ICMATE)

e-mail: enrico.miorin@cnr.it

Mail address: Corso Stato Uniti, 4 - 35127 Padova, Italy

Phone: +3904982958770

ABSTRACT

Environmental barrier coatings are necessary to withstand harsh operating conditions in several industrial fields. Depending on the type of application, it is becoming mandatory to develop an effective screening procedure to identify the most performing film/substrate system. Within this general framework, the present research work objectives are: i) to investigate the process-structure-property correlations in titanium aluminum nitride (Ti-Al-N) coatings on γ-TiAl-based substrates and to improve their performance in oxidizing atmosphere; ii) to identify an effective method to rapidly optimize the best film/substrate architecture.

The same optimized Ti-Al-N coating was grown via reactive High Power Impulse Magnetron Sputtering (HiPIMS) technology on three Ti-48Al-2Cr-2Nb billets characterized by different surface pre-treatments before depositions: surface polishing, surface polishing combined with a strong plasma etching, and surface polishing coupled to both a weak plasma etching and a Ti-Al metallic interlayer deposition. Then, all the specimens were cyclically treated up to 200 cycles at 950 °C, using a Burner Rig (BR) facility.

The chosen Ti-Al-N/substrate interface design considerably influenced average compressive residual stress (S_{res}) and adhesion of just deposited films. Moreover, it was possible to identify a clear relationship between S_{res} behavior and each coating performance after BR tests. It became clear that the weak plasma etching/Ti-Al interlayer match helped improving the system stability (i.e. very low average residual stress thermal relaxation) thus guarantying high temperature oxidation resistance.

KEYWORDS

Film-substrate interface design; Reactive HiPIMS; TiAlN coatings oxidation resistance; γ-TiAl based alloys; Residual stress; Burner-rig thermal test.

1. INTRODUCTION

Environmental barrier coatings play an increasingly central role to withstand harsh operating conditions in several fields. Furthermore, depending on intended application, it is becoming more and more demanding to develop a preliminary testing procedure to screen and select a suitable film/substrate architecture. Within this general framework, the present research work goals are: 1) to deposit Ti-Al-N coatings via reactive HiPIMS on γ-TiAl-based substrates while changing the interface design in order to enhance resistance to challenging thermal cycling treatments in oxidizing atmosphere; 2) to try to figure out an effective testing method to identify the most likely film/substrate interface design.

γ-TiAl-based alloys, thanks to their unique combination of low weight and good mechanical properties, are very attractive to industry for a wide range of applications, such as turbine blades in aero-engines, power-plant turbines and turbocharger rotors in automotive engines [1]. Despite this, with the aim of using these materials at high temperatures, further oxidation protection capability is mandatory. A severe oxidation starts is within the range between 750 °C and 850 °C, depending on the alloy chemical composition. The bare material forms a non-protective scale made of mixed oxides, since thermodynamic stabilities of alumina and titania are virtually identical [2, 3]. Apart from the temperature, other aspects such as environment, surface finishing and microstructure are fundamental for the oxidation comportment [4, 5, 6]. The most likely methodology to protect γ-TiAl-based alloys against environmental failure is *surface engineering* that, in this specific case, entails the formation of protective surface oxide scales (such as α-Al_2O_3, Cr_2O_3, SiO_2, or a combination thereof) that inhibit diffusion of oxygen (and/or other aggressive species) into the substrate, thus preventing the bulk material deterioration. As described in detail in [6], different kinds of films have been investigated in the past. Not only the coating must endorse the formation of a compact and stable oxide layer,

but also it must be well adherent to the substrate, since zones that are most inclined to degradation are located at the interfaces coating/environment and coating/substrate.

Keeping in view the previous considerations, for this research work, Ti-Al nitride overlay coatings were chosen and grown via reactive HiPIMS technology. In terms of material, Ti-Al-N is well-known and used both for laboratory and industrial applications; moreover, it shows a good chemical compatibility with the γ-TiAl substrate permitting to avoid a rapid degradation of the system due to diffusional losses into the substrate material and vice versa [7]. Furthermore, the similarity of the coefficients of thermal expansion (σ) between the coupled materials (i.e. the mechanical stability of the system in case of temperature changes) was considered too (σ(Ti-Al-N)=7.5x10^{-6} K^{-1} [8]; σ(TiAl substrate)=10x10^{-6} K^{-1}, according to performed measurements). Therefore, for our purpose it represents an optimum candidate film for this type of substrates.

Concerning the deposition technology, HiPIMS produces an ultra-dense plasma [9, 10] leading to high-density coatings [11] with enhanced adhesion [12] especially for complex-shaped surfaces [13], improved toughness, reduced columnar structure and deposition temperature [14]. Hence, an optimized Ti-Al-N coating was deposited on three γ-TiAl-based billets after modifying progressively film/substrate interfaces to improve its performance: mechanical polishing, surface polishing combined with a strong plasma etching, and mechanical polishing coupled to both a weak plasma etching and a Ti-Al metallic interlayer deposition. Then, all the specimens were cyclically heat treated using a burner rig facility [15] and analyzed after 40 cycles at 850 °C, 100 and 200 cycles at 950 °C.

In other words, three substrate treatments before depositing the same optimized Ti-Al-N film were performed to enhance the overall resistance to repeated thermal cycles. Each surface finishing had a strong influence on Ti-Al-N coating growth and its chemical/physical properties: morphology, microstructure, residual stress, mechanical behavior and adhesion, as

well as oxidation resistance. In particular, a clear correlation between interface status, coating average residual stress and film/substrate system oxidation behavior was identified. Thus, it was possible to individuate an effective route to provide reliable information on the oxidative behavior of each protective architecture, even after the blandest cycling thermal test.

2. EXPERIMENTAL DETAILS

2.1 Film deposition

Bars of Ti-48Al-2Cr-2Nb alloy (diameter = 25 mm) were processed by electron beam melting and then thermally treated. The production technique was described elsewhere [16]. Several 15 mm high disks were cut from these rods. Their top surfaces were polished to a 1 μm diamond finish before depositing Ti-Al-N coatings by reactive HiPIMS. For each sputtering run, three identical substrates were located in the vacuum chamber to carry out subsequent thermal tests and chemical/physical characterizations on equivalent samples. Based on preliminary results, all the TiAl nitride coatings were deposited using optimized working conditions (displayed in Table I). All depositions were accomplished using a turbo-molecular pumped high-vacuum cylindrical vessel, which was previously evacuated to a base pressure lower than $1x10^{-5}$ Pa. Ar inert gas (99.9997% purity) and N_2 reactive gas (99.998% purity) were injected through mass flow controllers to achieve the selected pressure and the right mixture of sputtering gases. A TiAl target (1:1 at. %, about 10 cm in diameter, 6 mm thick, and 99.9% purity) was mounted on a magnetron cathode, driven by a HiPIMS power supply (TRUMPF-Hüttinger, True Plasma High Pulse 4002). For the substrate biasing, an 18 kW special unit model 3018 HBP (TRUMPF-Hüttinger) was employed. The substrates were positioned 100 mm below the cathode, maintaining the face to be coated parallel to the target surface. They were heated at 400 °C before the sputtering run and temperature was maintained throughout the process by *ad hoc* heaters and a proper thermocouple monitoring.

Table I: HiPIMS working parameters set for Ti-Al-N film depositions.

HiPIMS working parameters	
Power (average value) [W]	1000
Pulse length [μs]	25
Frequency [Hz]	500
Gas	Ar + N_2 (50%)
Pressure [Pa]	1.0
Substrate bias voltage [V]	-50
Duration [min]	180

The film/substrate interface was progressively modified in an attempt to affect performance. Therefore, three kinds of Ti-Al-N samples were processed adopting different methods for Ti-48Al-2Cr-2Nb intermetallic alloy surface preparation. Films Sm (i.e. Smooth) were only ultrasound cleaned before the coating deposition. In Et (i.e. Etched) specimen case, besides ultrasound cleaning, a 60 minutes plasma etching was performed too. Literature has shown that using HiPIMS, target metal ions bombard the substrate leading to elimination of contaminants, creation of intermixing zones, and the growth of crystalline metallic interlayers, which could increase the coating/substrate adhesion [17]. Anyway, several critical factors were identified [18]: 1) the capacity to form interlayers and intermixing regions depends on the second ionization energy of the metal used for the HiPIMS pretreatment; 2) the intermixing area role is unclear; 3) a noteworthy adhesion is not only determined by the presence of an interlayer; 4) it is necessary to consider the bonding nature; etc.. In view of the above, the plasma etching step was carried out maintaining the TiAl target at a low average power (100 W) and applying a 1200 V bias voltage to the sample holder (Ar pressure 1.0 Pa, frequency 500 Hz, pulse length 25 μs). In these conditions, ions reaching the substrate were predominantly Ar ions, since the fraction of ionized metal flux depends on applied power [17].

Finally, for samples labelled Il, the pre-treatment duration was reduced from 60 to 10 minutes and a Ti-Al metallic interlayer (from which the acronym Il) was interposed between the substrate and the nitride coating. Selected working parameters were the same depicted in Table I with the exception of deposition duration (10 minutes) and process gas (pure Ar).

2.2 Burner-rig test

The uncoated specimens as well as the coated ones were tested, using a *burner rig* (BR) apparatus. The burner rig facility [19] was specifically designed to investigate materials under simulated operating conditions experienced by structural components of hot parts of turbines,

and allowed testing twelve specimens simultaneously, in the same experimental conditions. This apparatus granted very quick temperature variations by using a flame, fed by methane and air, oriented towards the samples. The true thermal history of each sample was recorded through thermocouples placed near the sample surface. The testing temperature was computer controlled based on the average temperature experienced by each specimen.

The samples were subjected to transient test conditions, in terms of both temperature and oxidizing atmosphere, according to a three-steps thermal cycling. Each cycle consisted of a fast heating step up to a predefined maximum temperature, an isothermal step at the maximum temperature and an air-quench final step. The flame heated the samples up to the pre-fixed temperature in ten-fifteen minutes, and then the fuel/air supply was tuned in order to keep the average temperature of the specimens constant for 3 minutes. Finally, the flame supply was reduced to a minimum and, at the same time, every sample was hit by a dedicated airflow to decrease the temperature down to 300 °C in two minutes. The flame was fed by using air in excess with respect to the stoichiometry of the combustion reaction (17:1 air to fuel volume ratio during the isothermal step).

Thermal cycling of uncoated intermetallic alloy and Ti-Al-N/Ti-Al systems was repeated 40 times up to 850 °C, 100 and 200 times up to 950 °C. Oxygen concentration variations in the burner rig atmosphere, occurring during each cycle could be calculated considering the fuel to air volume ratio and assuming a complete methane combustion. At the beginning of each cycle, i.e. after a quenching step, the burner rig chamber was filled by air (21% vol. of oxygen). Then, the oxygen concentration progressively decreased during heating and isothermal steps (down to 8.7%), and finally it quickly increased again during the final quenching step.

2.3 Film characterization

2.3.1 Morphology, composition and crystal structure

Film morphology and chemical composition were analysed by a Sigma Zeiss field emission scanning electron microscope (FE-SEM), equipped with an Oxford X-Max energy dispersive spectroscopy (EDS) system. Coating thickness was evaluated by means of the ball crater micro-abrasion method [20, 21] (Anton Paar Calotest, plus Image J software [22]). Profilometric analyses were performed through the Leica DCM 3D profilometer (LeicaMap software) according to ISO 25178 and ISO 4287 standards [23, 24]. The crystal structure was evaluated by X-ray diffraction (XRD) with a Panalytical X'PERT PRO PW3040/60 diffractometer operating in Bragg-Brentano geometry and equipped with a Cu-Kα source (Micro-XRD Rigaku D/max probe 100 micron). Diffractograms were first evaluated with the Match! 2.2.1 Software, to identify the crystalline phases from the position of detected peaks.

2.3.2 Mechanical properties

Elastic modulus (E) and hardness (H) of Ti-Al-N coatings were measured by instrumented nanoindentation testing as widely described by the authors in [25]. Concerning Poisson's ratios, a value of 0.25 was chosen for the Ti-Al-N material (which is a typical value for nitride PVD coatings), and a value of 0.3 for the substrate.

H and E results are obtained after averaging over 20 different tests within the depth range of 100-120 nm, in order to minimize substrate's related artifacts. A full calibration of area function and frame stiffness was performed before and after each series of measurements, by using a certified fused quartz reference sample.

2.3.3 Adhesion

The adhesion properties of the Ti-Al-N/Ti-Al systems were evaluated with scratch tests using an UMT-2 tribotester (Bruker), provided with a standard Rockwell C diamond tip. Test parameters were selected referring to UNI EN 1071-3 standard [26] for ceramic materials in PLST (progressive loading scratch test) mode. The coating adhesion was quantified measuring the critical load Lc3, at which the coating delamination occurs. Lc3 was estimated

by combining recorded signals (normal and lateral forces, acoustic emission) with SEM and optical images of scratch tracks.

2.3.4 Average residual stress

The coating's residual stress was investigated using the Focused Ion Beam (FIB) micro-scale incremental ring-core method, a material removal technique that allow measuring local residual stress with sub-micrometer spatial resolution. The procedure involves FIB incremental milling of a micron-size annular trench (Fig. 1) of increasing depth, in combination with high-resolution in-situ SEM imaging after each milling step and a full field Digital Image Correlation (DIC) analysis for relaxation strain evaluation [25, 27, 28].

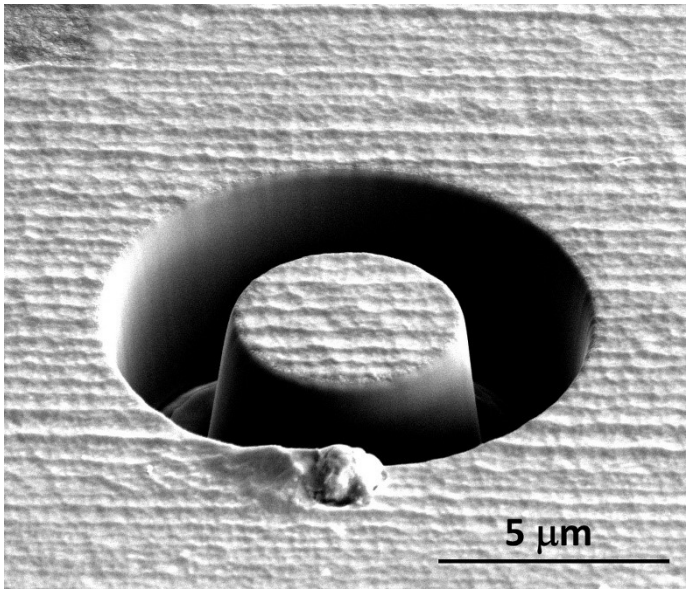

Figure 1. A test performed on a Ti-Al-N coating deposited on a γ-TiAl based substrate. The residual stress in the central stub (~ 5 μm inner diameter) is progressively relaxed as the depth of the trench increases, thus giving measurable strains on the top surface. They are calculated from the SEM micrographs by a specifically developed DIC procedure. Microstructural features over the surface are sufficient to guarantee a very accurate displacement measurement.

3. RESULTS

3.1 Morphology and composition

The Ti-48Al-2Cr-2Nb intermetallic substrate has a *duplex* microstructure, which ensures an optimum strength, ductility and fracture toughness compromise. As extensively described elsewhere, it is produced using a proper Ti:Al atomic ratio together with a specifically designed thermal treatment [29]. The dual phase microstructure consists of regions showing fine lamellar colonies consisting of cubic γ-TiAl and hexagonal α_2-Ti_3Al phases and areas mainly containing equiaxed gamma grains. The average chemical composition, measured by SEM-EDS, was: 51 at.% Ti, 45 at.% Al, 2 at.% Cr, 2 at.% Nb.

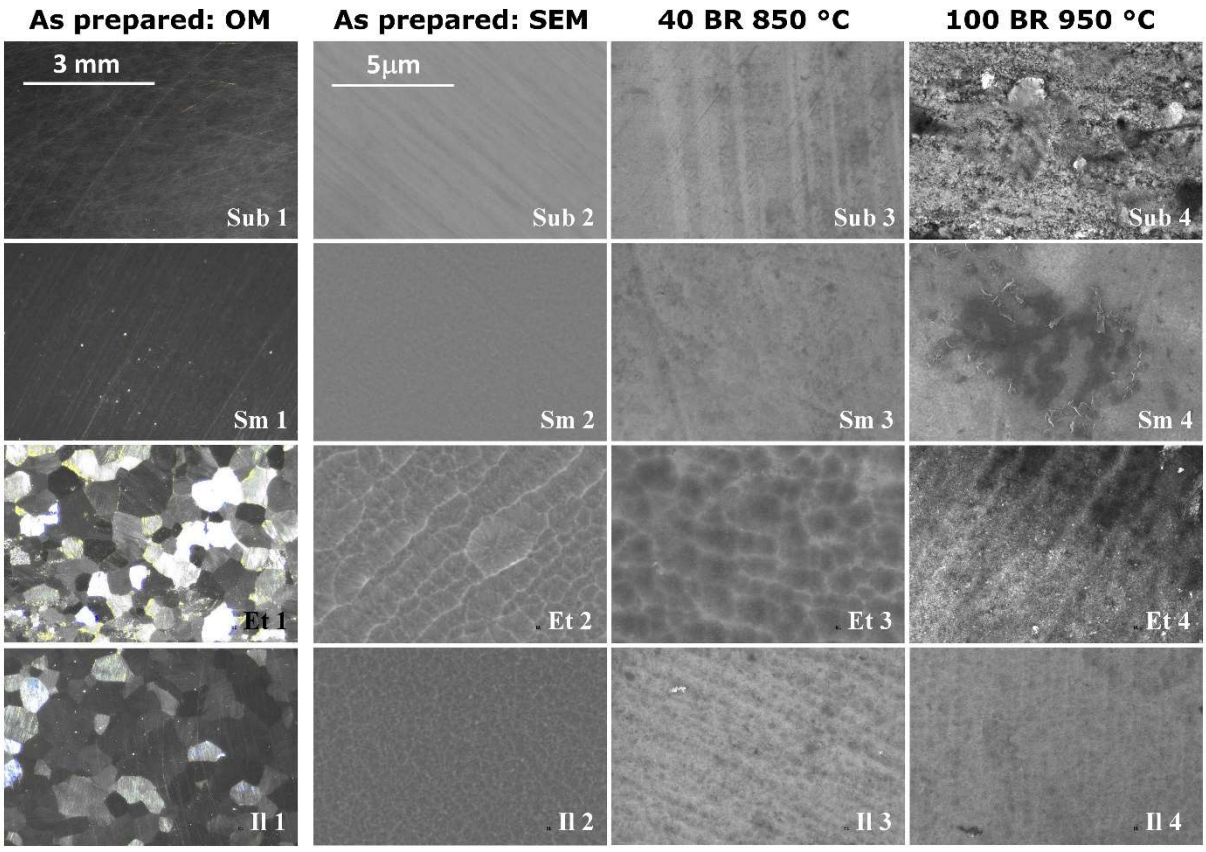

Figure 2. γ-TiAl based substrate (Sub 1, 2, 3, 4) and Ti-Al-N coatings optical microscope (OP) and SEM images just after deposition, after 40 BR cycles up to 850 °C and 100 cycles up to 950 °C. Sm films were flat, compact and uniform; Et layers clearly reproduced the substrate solidification structure highlighted by the strong plasma etching; Il coating still

allowed seeing the billet solidification structure. After the 850 °C test, no obvious differences between the three HiPIMS samples could be detected. After 100 cycles up to 950 °C, type Et films were discarded; Il coatings were morphologically quasi-intact.

As deposited Sm coatings surface examination indicated they were flat (mean roughness R_{aSm}~10 nm, thanks to the smooth polished substrate surface) compact and uniform. Only a few defects were detected consisting of sporadic macroparticles due to the rare arches recorded during the sputtering process (Fig. 2 Sm1). The Ti:Al atomic ratio (SEM-EDS) was equal to 1 (58 at.% N, 21 at.% Al, 21 at.% Ti). Coating Et perfectly reproduced the substrate morphology too: indeed, the strong vacuum plasma etching treatment completely removed the plastically deformed surface layer obtained after cutting and mechanical polishing procedures and, thanks to different erosion speeds of adjacent grains, it highlighted the substrate solidification structure (Fig. 2 Et1). Moreover, on a microscopic scale (Fig. 2 Et2), the high-energy ion bombardment produced an obvious morphology modification of the film: samples Et were less homogeneous and rougher, showing R_{aEt}~130 nm. When considering Il, the weak plasma etching lasting for 10 minutes together with the interposition of a 300 nm thick Ti-Al metal layer, still allowed the exposure of the billet solidification structure (Fig.2 Il1). The microscopic scale morphology detected by SEM analysis (Fig. 2 Il2) was close to Sm specimen one, the roughness was low, with R_{aIl}~30 nm.

After the 850 °C burner rig test, corresponding to a *mild treatment* (Fig 2 Sm3, Et3 and Il3) the three HiPIMS samples surface morphology started changing from the initial state because of the growth of an oxide layer that progressively hid the underlying nitride coating. Turning to SEM-EDS, the average atomic percentage of nitrogen oscillated between 37 and 39, the oxygen one between 25 and 27, aluminum and titanium were at 17-18 at.%.

During the following burner rig tests, the peak temperature was raised up to 950 °C, which could be considered a very harsh condition since the severe oxidation of γ-TiAl based alloys starts between 750 °C and 850 °C. Moreover, the number of burner rig cycles was increased up to 100 and 200, trying to achieve the complete failure of the coatings. After 100 cycles up to 950 °C (Fig. 2 Sm4, Et4, Il4), type Et films were discarded because they did not yield satisfactory results (see the following paragraphs too). After such severe tests, not only the two remaining specimens were still present and perfectly adherent to their substrates, but also Il coating was morphologically quasi-intact. Therefore, just at the final challenging test, morphological/compositional characterizations permitted to identify Il as the most promising sample.

3.3 Microstructural characterization

3.3.1 X-ray diffraction

The XRD patterns were collected from samples in the as-deposited state and after thermal treatments at both 850 and 950 °C. As expected, the XRD spectrum of the substrate alloy showed the typical peaks of a bi-phasic crystal structure, constituted of tetragonal γ-TiAl and hexagonal α_2-Ti_3Al phases. As the thermal treatments temperature raised, an evolution of the structure towards the increase of γ phase content was observed [15]. The amount of γ phase changed from about 68% weight fraction in the as received state, to 83% after 40 cycles up to 850 °C, until 89% after 200 cycles up to 950 °C.

The γ-TiAl phase showed a preferred growth in (111) plane and such texture has been reported in some previous studies too [30, 31]. TiAl alloys exhibit a dendritic microstructure, in which α-dendrites are transformed, after solidification, into a lamellar microstructure with a preferred orientation of the lamellae, thus <111> fiber texture is due to the planes of the aligned lamellae. This status persisted also after the most onerous thermal treatment, with a

slight growth of peaks (002) and (200), located respectively at 44.8° and 45.5° on 2θ axis, probably due to dynamic recrystallization phenomena (Fig. 3).

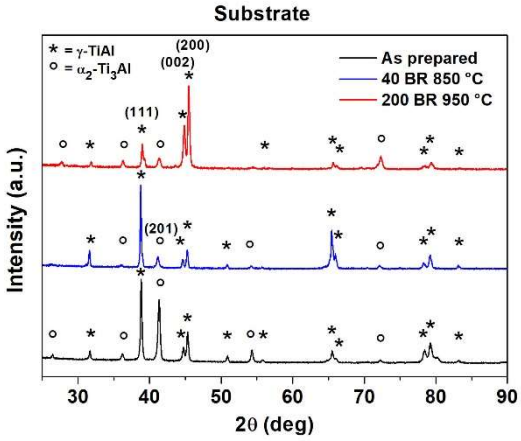

Figure 3. XRD patterns collected from substrates in the as received state and after burner rig treatments (40 cycles up to 850 °C and 200 cycles up to 950 °C).

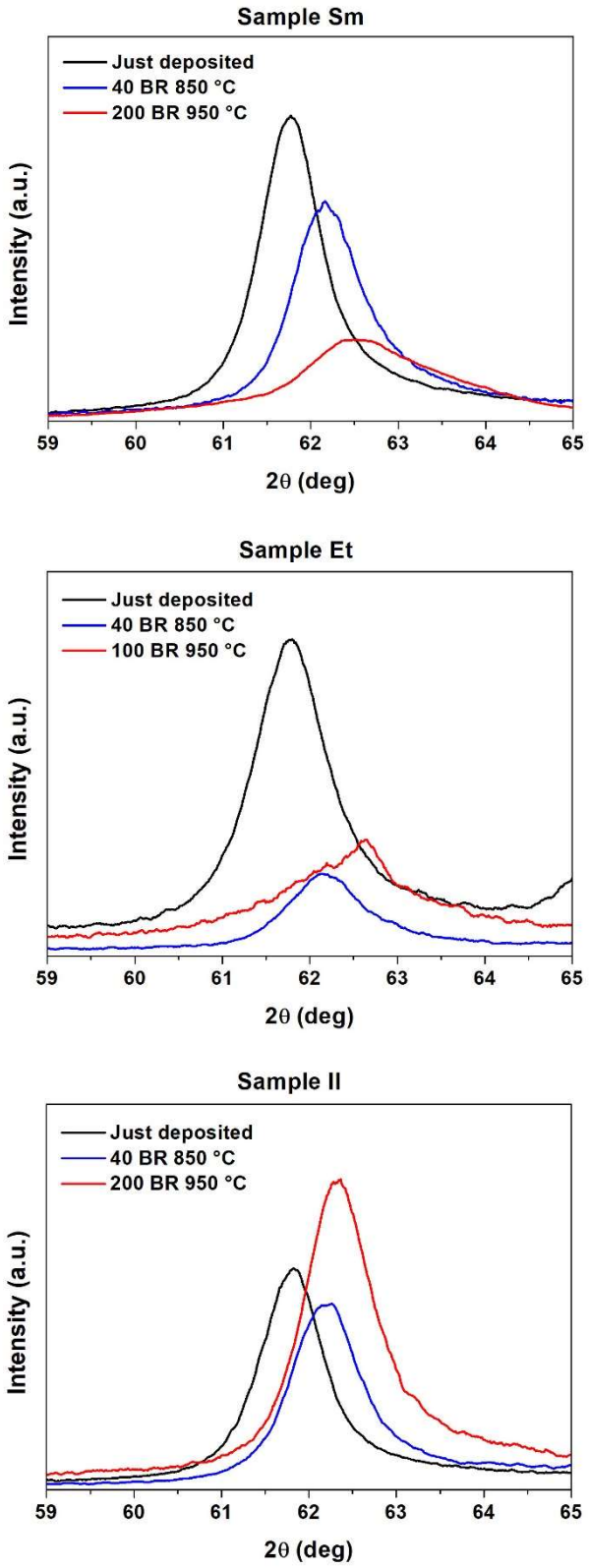

Figure 4. Normalized Ti-Al-N (220) peaks in XRD analyses performed on samples Sm, Et and Il.

In the XRD spectra of coated specimens, only a single intense and broad signal was detected at 2θ ≈ 61.8°, corresponding to (220) peak, attributable to a mixed nitride of Ti and Al (1:1), with a face-centered cubic crystal structure (Fig. 4). It was indexed with the solid solution (Ti, Al)N phase, derived from TiN cubic structure and having space group Fm-3m [32, 33, 34]. One could imagine that a high Al fraction may distort the B1 fcc structure of TiN [35]. XRD texture analyses were performed with a texture goniometer. Measurements were accomplished by fixing the 2θ angle, thus maintaining constant d-spacing, and moving the sample through χ (tilt) angles and φ (spindle) rotations. Then, measured intensities were plotted as an intensity map where the hemisphere-like distribution of scattered intensity was projected on a 2D "pole figure", showing the variation of intensity with sample orientation. Fig. 5 reports the (220) pole figure, collected at 2θ=61.8° for sample Sm (shown as an example), according to the peak position of (220) plane in the XRD diffraction pattern. A [110] fiber texture was exhibited.

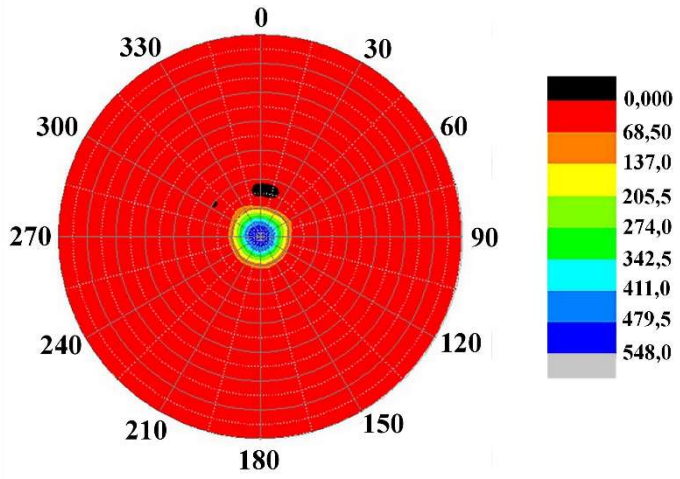

Figure 5. (220) pole figure collected from sample Sm.

In fact, magnetron sputtering based technologies are known to cause sturdy coating texture. The orientation of films is intensively influenced by ion bombardment during film growth. Studies have shown that for face-centered cubic materials the (110) orientation is expected

because of ion channeling. In other words, the (110) crystalline planes survive under the concurrent ion bombardment due to a lower resputtering rate. Therefore, (110) texture may simply be a result of crystal alignment through energetic ion bombardment, i.e. particle energy is sufficiently high and the ion channeling becomes dominant [36, 37].

The burner rig tests carried out at 850 °C for 40 cycles or at 950 °C (100 and 200 cycles) did not lead to the presence of oxide peaks in the XRD collected spectra, thus confirming that a very thin or amorphous oxidized layer formed under the achieved harsh conditions, which could not be detected because of the technique limitations. Furthermore, the (220) Ti-Al-N peak remained still visible in all the XRD spectra.

As stated above, focusing on the (220) peak position of as deposited films, they were found at about 61.8° for all samples. Therefore, knowing (Ti,Al)N (Ti:Al = 1:1) reference peak is located at $2\theta = 62.6°$, they appeared shifted towards low angles. The peak position depends on the nitride composition, as mentioned before, and on possible residual stresses as well. An interpretation of this behavior is proposed in the Discussion section. Moreover, the peak attributed to the nitride phase changed its position after burner rig towards higher 2θ values. The peak movement was found to be very similar for samples Sm and Et, reported respectively in Figure 4(a) and 4(b), and the maximum peak shift was estimated as almost 1° on 2θ axis for both specimens. Figure 4(b) shows the XRD spectrum of burner rig treatment after 100 (in lieu of 200) cycles up to 950 °C because sample Et revealed not to be able to withstand the most severe treatment. Finally, for sample Il, the nitride phase peak remained approximately in the same position, with a maximum shift of about 0.4° on 2θ axis. In conclusion, the only X-ray diffraction technique did not allow obtaining conclusive and unambiguous information about the HiPIMS nitride coatings because just a single peak was attributable to the (Ti, Al)N phase. The only evidence was that, despite the same crystal structure and composition, Il coating showed a different behavior.

3.3.2 SEM–FIB investigation

The FIB analyses confirmed the formation of an oxide layer and permitted making comparisons between bare and coated specimens (Table II, Fig. 6). Measured thicknesses were similar for the three coatings and constant all over the samples surfaces. They ranged from 2.2 to 2.4 μm. FIB characterizations clearly revealed microstructural modifications (Fig. 6 a, b, c). Sample Sm film-substrate interface showed typical small grains which rapidly evolved into competitive columnar growth at thickness <100 nm (Fig. 6 a). Instead, Il coatings exhibited a transition layer (about 500 nm thick), above the interlayer, exhibiting a low pronounced columnar growth with nearly equiaxed grains (Fig. 6 c). Therefore, it could be assumed the addition of the Ti-Al metallic film resulted in a continuous renucleation step, which was not observable in the other two cases.

Concerning coating Et, (Fig. 6 b) during γ-TiAl intense pretreatment process, ionized argon bombardment induced sputtering of the substrate surface material leading to a rougher surface structure that helped creating *oblique deposition angles* (i.e. more defects) [38].

As expected, the higher the working temperature and the number of burner rig thermal cycles, the higher the thickness of the oxide scale on the surface of each sample (Table II, Fig. 6). In any case, the first important result was accomplished. Indeed, Ti-Al-N protective coatings had a clear beneficial effect since the oxidized layer was thinner than the one measured for the bare TiAl substrate. Comparing data from the three coated specimens, Sm seemed to give the best results at low temperature (up to 850 °C). Indeed, FIB test was not able to provide a thickness value of the oxide layer. On the one hand, the scale was very thin and the initially formed flake was not coherent. Proceeding with the cycling heat treatments (> number of cycles and/or > working temperature), Il coating proved to be the most stable protective layer: not only the oxide film thickness was small, but also it remained almost constant despite the

worsening of the test conditions. Depending on the film properties and burner rig treatment, the oxide layer looked dense and compact or porous (Fig. 6).

Table II: Oxide scale thickness (standard deviation ± 5 nm) before and after BR cycling thermal treatments from FIB sections.

Sample	Oxide thickness (nm) 40 BR 850 °C	Oxide thickness (nm) 100 BR 950 °C	Oxide thickness (nm) 200 BR 950 °C
Bare γ-TiAl	192	296	581
Sm	/	95	243
Et	137	306	/
Il	50	53	95

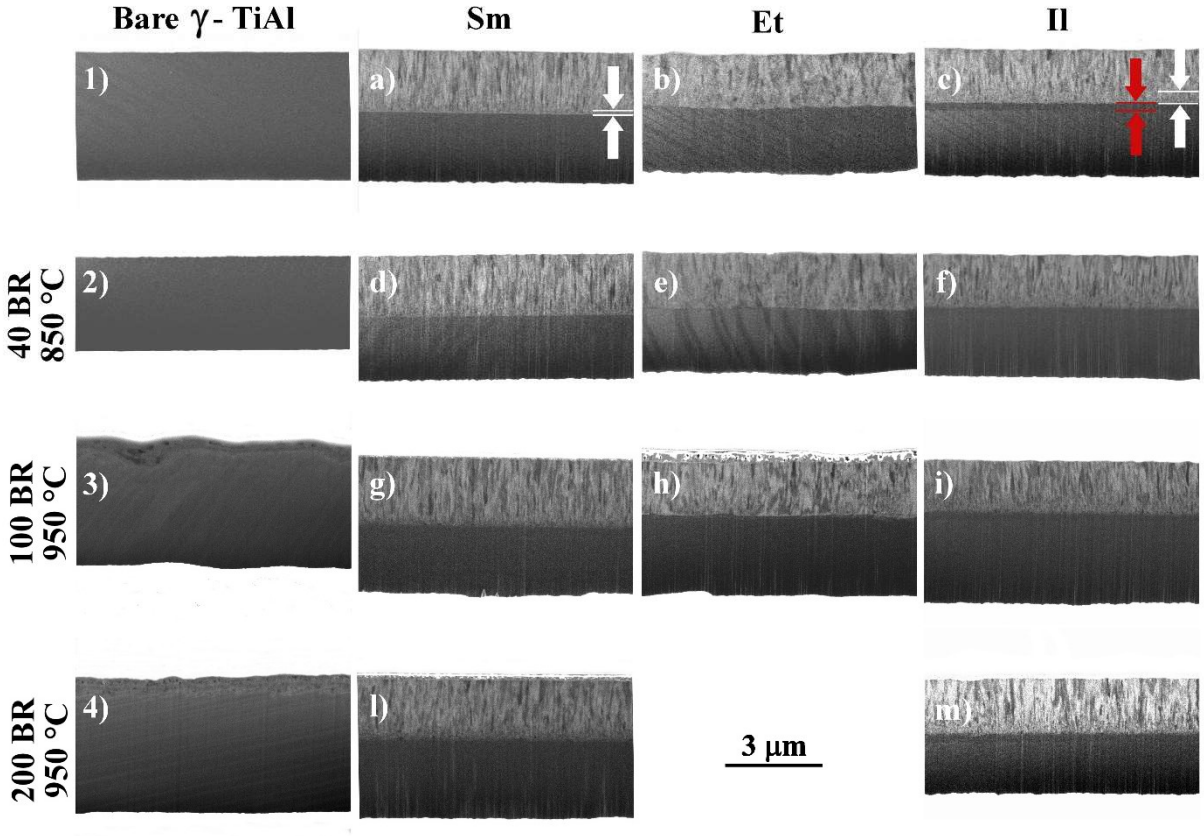

Figure 6. FIB images of the oxidized surfaces: the oxide scale was analyzed after each burner rig treatment. After 40 cycles up to 850 °C, it was not possible to measure Sm oxide film thickness: it was very thin and incoherent. Sample Et was not investigated up to 200 cycles at 950 °C: its behavior was comparable to bare TiAl one, already after 100 cycles up to 950 °C. In a) and c) the *small grain* layer is highlighted (white lines and arrows); in c) the Ti-Al metallic interlayer is shown too (red lines and arrows).

By way of example, FIB cross sections after 100 cycles at 950 °C could be described (Fig. 6 3, g, h, i). For TiAl intermetallic bare alloy, the oxide layer was well evident (~ 300 nm) and spongy (black holes were clearly visible). Sm oxide scale was visible and slightly porous while porosity became obvious for Et (thickness > 300 nm plus big dark holes). Finally, considering Il coatings, the oxide film was very thin (~ 50 nm) and appeared solid. After 200 cycles at 950 °C the oxide scale remained small and dense only for type Il specimens. FIB observations confirmed that film/substrate interfaces generally looked sharp and free of

defects. Analyzing Et section view after 100 cycles up to 950 °C (Fig. 6 h), a small detachment was visible. In summary, sample Il presented a thin and compact oxide layer irrespective of the performed burner rig treatment. Hence, it was designated as the most stable HiPIMS coating.

3.3.3 Scratch tests

Scratching tests allowed assessing film/substrate adhesion strength for as deposited samples and after 40 burner rig thermal cycles up to 850 °C. The scratch behavior of sample Et was difficult to interpret due to the peculiar topology of its surface (Fig. 2). As indicated in Table III, the mild plasma cleaning followed by the inter-deposition of a Ti-Al glue layer evidently enhanced the film/substrate adhesion properties, exhibiting a ~ 30% Lc3 increment. Such increase could result from the accommodation, due to the presence of Ti-Al, of the stresses induced by the indenter.

The burner rig treatment did not promote any critical load change for sample Sm, while it slightly weakened film/substrate adhesion for specimens Il (Fig. 7).

Table III: Ti-Al-N film/substrate adhesion results.

Sample	Lc3 Critical Load (N)	
	As deposited	After 40 cycles at 850 °C
Sm	-35±1	-36±1
Il	-47±3	-43±3

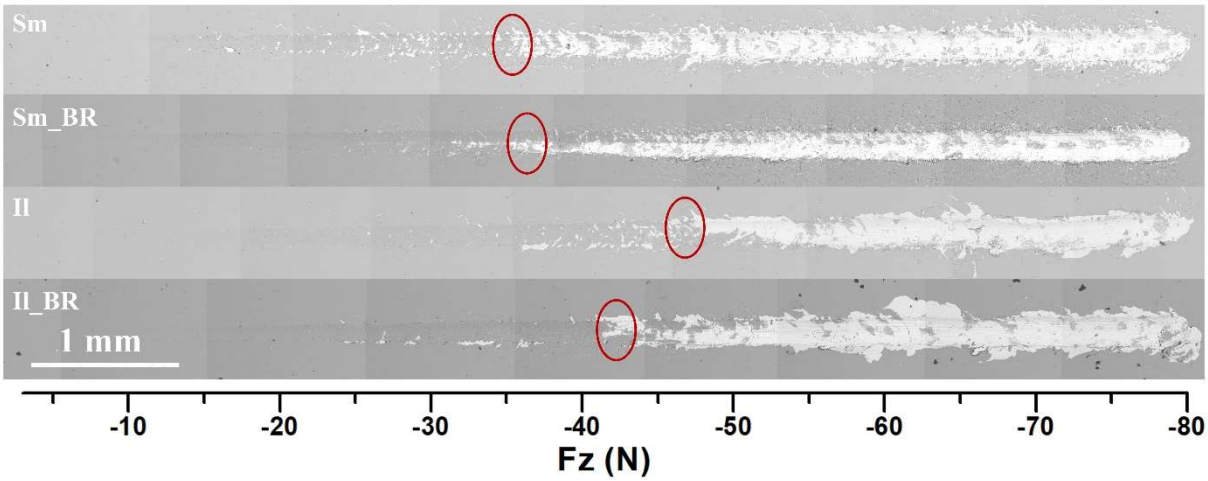

Figure 7. SEM micrographs of progressive loading scratch tests concerning samples Sm and Il, before and after 40 burner rig cycles at 850 °C. Failure points were highlighted by red circles.

Concerning sample Et, the aggressive plasma etching treatment performed for it (60 minutes, -1200 V) strongly affected the coating response to scratch test due to the net steps between adjacent grains that brought to a wide dispersion of Lc3 results. Therefore, Lc3 values could not be confidently associated to the true film/substrate adhesion.

3.4 Mechanical properties

Hardness (H) and elastic modulus (E) of the bare TiAl alloy together with film/substrate systems mechanical properties were measured before and after burner rig thermal treatments (calculation depth 100 – 120 nm).

TiAl substrate's hardness was found to be (7.8 ± 0.3) GPa. Instead, considering coated samples, their nano-hardness was notably higher and ranged between 30 (Et coupon) and about 35 GPa (Fig. 7). Concerning sample Et, data spread was significant and probably due to its relatively high surface roughness (R_{aEt} ~ 130 nm).

Analyzing coated specimens case, after 40 burner rig cycles up to 850 °C, a clear H value decrease was detected. As observed via FIB (Fig. 6) and confirmed by XPS data [15, 19] (not

shown here), a thin oxide layer was already present at this stage. Therefore, this hardness drop could be associated (at least in part) to the formation of the first oxide scale, in all cases (see also Discussion section).

After subsequent thermal treatments, hardness value further decreased only for samples Sm and Et, while it kept constant for Il specimen. After the initial variation, coating Il surface layer properties remained almost unchanged confirming that a very dense and stable oxide layer was formed and could behave as a protective scale during the subsequent BR tests. This was validated further by the elastic modulus values that were measured within the same nanoindentation experiments. Film Et average modulus, correlated to density [39], was slightly lower than that of the other coatings and the corresponding error bar was very large denoting a huge sample inhomogeneity. A high modulus was measured for Il sample, even after 200 oxidation cycles at 950 °C while a clear decrease of it was observed for the other two specimens (Fig. 8).

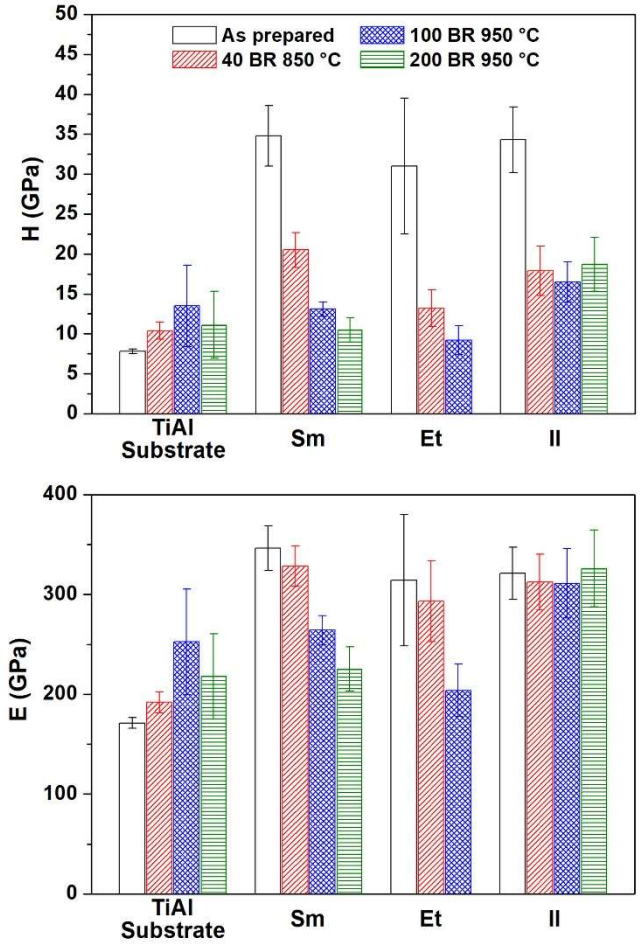

Figure 8. Hardness (H) and elastic modulus (E) measured before and after burner rig thermal treatments (calculation depth 100 nm)

Finally, considering TiAl intermetallic alloy, after an initial H increase (the grown oxide is harder than the substrate) measured values remained constant within experimental error. It was also easy to note a higher nanoindentation data scatter, which is a typical artifact related to the increase of surface roughness due to the incoherent Ti/Al oxide layer growth. The elastic modulus of the TiAl substrate was equal to (171 ± 5.2) GPa. Instead, coated samples modulus was much higher and always greater than 300 GPa.

3.5 Average residual stress

Ti-Al-N coatings average residual stress was measured before and after different BR heat treatments using the focused ion beam (FIB) micro-scale incremental ring-core method (as described in 2.3.4).

Table IV: Average residual stress measured before and after burner rig cycling heat treatments using the focused ion beam (FIB) micro-scale incremental ring-core method. Standard deviations are estimated values based on the interpolation of strain curves.

	Residual stress S_{res} (GPa)		
	Sm	Et	Il
As Deposited	-5.5 ± 0.5	-7.7 ± 0.7	-6.6 ±0.4
40 BR 850°C	-4.3 ± 0.3	-4.5 ± 0.3	-5.9 ± 0.4
200 BR 950°C	-3.2 ± 0.2	/	-6.1 ±0.6

As shown in Table IV, compressive residual stress (S_{res}) were observed in all cases for as deposited coatings, but their values ranged from -5.5±0.5 GPa to about -7.7±0.7 GPa. Therefore, average residual stress levels clearly changed while modifying just the substrate surface treatment performed before the nitride film growing. The highest S_{res} (-7.7±0.7 GPa) was found for Et specimen.

In all coatings, residual stress relaxations (i.e. recovery and/or adhesion loss) after burner rig cycles were observed. However, the observed S_{res} reduction $\Delta\% = \frac{|(S_{res}1 - S_{res}2)|}{|S_{res}1|} x100$ was significantly different on the three samples under investigation. This was a strong indication that Δ% could be a useful microstructural parameter to identify coatings' thermal stability. Comparing S_{res} data before and after 40 burner rig cycles at 850 °C, the minimum Δ% = 10% was observed for Il coating while, sample Et was characterized by the most evident oxidation and higher Δ% (42%). Moving forward with BR tests, Sm and Il films were heat treated up to 200 cycles at 950 °C. For Sm, compressive residual stress relaxed considerably increasing temperature and the number of thermal cycles while, Il S_{res} values remained quasi unchanged (Δ% = 4%). Therefore, according to the obtained results, reported in Fig. 8, it was possible to assume that sample Il was the most stable and resistant to thermal cycling, since S_{res} remained approximately constant, regardless the severe heating treatments performed. Whatever the cause (coating microstructural modifications, adhesion loss, etc.), average residual stress relaxation is undoubtedly related to high temperature oxidation behavior. In addition, average residual stress evaluations seemed to allow discriminating between the three interface architectures, already after a mild burner rig test (40 cycles up to 850 °C).

4. DISCUSSION

Three identical Ti-Al nitride films were deposited via HiPIMS on three undistinguishable substrates, progressively modifying the interface design. Their high temperature oxidation resistance was clearly different as thoroughly described in previous sections.

The oxidation behavior of titanium aluminum nitride coatings was well investigated and reported in the literature. Generally, the oxide scale was found to consist of a double-layer structure, i.e. an Al-rich top-layer and a Ti-rich sub-layer below. Many authors attributed Ti-Al-N superior oxidation resistance compared to Ti-N to the dense Al_2O_3 top layer, which was expected to hinder the inward diffusion of oxygen [40]. Furthermore, it was reported that the mobile species are Al and O, whereas a limited mobility was detected for Ti [40]. Thus, the oxide scale grew by simultaneous outward diffusion of Al towards the oxide/air interface and inward diffusion of O to the oxide/nitride interface where Ti is oxidized. Other authors [41] found that increasing aluminum content the thickness of the oxide layer formed at 900 °C diminished. In particular, the Ti-rich sub-layer grew slower leading to reduced compressive stresses (i.e. less cracking probability of the protective Al-O based top layer) [41].

Here too, as previously pointed out in [15, 19], the authors could confirm a preferential diffusion of aluminum towards the sample surface. As expected, this Al surface enrichment phenomenon progressively occurred increasing temperature and/or the number of burner rig cycles (i.e. the oxide layer growth). Nevertheless the surface Al:Ti atomic ratio was very dependent on the coating/substrate design. In particular, after 200 BR cycles at 950 °C, the authors measured the surface concentration of Al (Al at.%) via X-ray Photoelectron Spectroscopy (XPS) and they found Al at. % : Ti at. % > 15 for sample Sm. Moreover, the aluminum accumulation at the scale surface also caused its diminution in the internal part of the oxide layer (corresponding to the mentioned Ti-rich sub-layer). Instead, sample Il showed an Al atomic percentage always higher than 20 at. % along the coating thickness. Proceeding

inward, only a small Ti at. % growth was observed (from 15 to less than 25 at. %). Therefore, even after the most severe BR test, sample Il still formed a Ti-Al mixed oxide followed by a Ti-Al-N plus oxygen layer (total thickness < 100 nm). In other words, in the case of Il specimen, even the harshest burner rig treatment performed for this research was not strong and/or long enough to allow the expected double-layer structure formation. Therefore, using the characterizations carried out, the authors tried to identify properties leading to such a different behavior. They also recognized measurable quantities that could help predicting high temperature oxidation resistance.

As reported in section 3.3.2, the Ti-Al metallic interlayer clearly promoted the growth of a fine equiassic cristallites layer at the early stages of film deposition. Hence, this microstructural peculiarity had a positive influence on high temperature oxidation resistance of this coating/substrate system. Furthermore, Il sample showed the best adhesion properties and the Lc3 superior value could certainly favor thermal stability too. Both microstructure and adhesion clearly affected average residual stress that varied considerably from case to case. In other words, interface design resulted in very different S_{res} values. This statement is reflected in the literature. Indeed, as already reported by Sprute et al. in [42], different substrate pre-treatments cause the introduction of diverse S_{res} levels within the substrate material and, as a direct consequence, they induce different residual stresses in the overlay coatings. For instance, grinding or ion-bombardment generally promote compressive residual stresses due to superficial plastic deformation (i.e. crystal lattice distortion). Therefore, the same Ti-Al-N coating material, which is supposed to have similar intrinsic residual stress, presents higher S_{res} in samples in which the substrates show higher residual stress due to performed pretreatment. It was reasonable to assume that sample Et (mechanical polishing plus strong plasma etching) had a major S_{res} than sample Sm (mechanical polishing) mainly for this reason.

Moreover, in [42] authors compared Ti-Al-N and Ti/Ti-Al-N deposited on substrates with the same pre-treatments before depositions and they measured a higher compressive stress for the multilayer system. This behavior was ascribed to thermal stresses, which are typical of PVD coatings because of temperature changes during depositions and differences on thermal expansion coefficients of the coating systems constituents. Indeed, generally, compressive residual stress develops in the material with the lower thermal expansion coefficient. This rule applied for sample Il (mechanical polishing, a soft negligible plasma etching, 300 nm Ti-Al glue layer) where metallic Ti-Al interlayer exhibited the higher thermal expansion coefficient ($> 12x10^{-6}$), increasing the compressive S_{res} in Ti-Al-N coating (Sm: 5.5±0.5 GPa vs Il: 6.6±0.8 GPa).

As reported in 3.5, in all coatings, residual stress relaxations after burner rig cycles were observed. These recovery effects resulted in a final measurable reduction (Δ%) of the overall average stress state of the material [43]. In this study, Δ% was significantly different on the three samples: after 40 BR cycles at 850 °C, sample Il showed the minimum Δ%, sample Et the highest. Coatings Sm and Il were heat treated up to 200 cycles at 950 °C: compressive stress relaxed further for Sm while, Il S_{res} values remained nearly unchanged. Therefore, sample Il, which was undoubtedly characterized by the best thermal stability, showed an intermediate average residual stress level together with the minimum Δ%. The following are some additional remarkable considerations concerning experimental results, which are useful to further strengthen the previous statement.

Regarding microstructure, XRD spectra collected from Ti-Al-N coatings were similar. Focusing on the (220) peak position of as deposited films, they were found at about 61.8° for all samples. Knowing (Ti,Al)N reference peak is located at $2\theta = 62.6°$, they appeared shifted towards low angles. As reported in various textbooks [44] and articles [45, 46, 47, 48] on XRD characterization technique, peaks shifts can be caused by macrostrain or by changes in

chemical composition and it is actually hard to separate the two contributes. Anyway, being the average residual compressive stress values very high for all deposited coatings (see paragraph 3.5), it was possible to assume S_{res} certainly gave a significant contribution to the observed shifts. In case of a thin layer, stress is roughly planar and XRD peaks in a typical theta-2theta scansion are shifted to lower angles for compressive stress and to higher angles for tensile stress. In other words, a simple biaxial compressive residual stress in the plane of a film leads to a lattice parameter increase in the direction perpendicular to the plane of the coating and, in a classical experiment, x ray diffraction measures the lattice parameter in this direction.

The XRD peak attributed to the nitride phase changed its position after thermal shock treatments, moving towards higher 2θ values (section 3.3.1). The peak movement was found to be very similar for samples Sm and Et (Fig. 4), and it could be construed as a relaxation of the coating internal macro-stress. Ti-Al-N coatings exhibiting the same crystal structure and very similar compositions should undergo a comparable change of the lattice parameter after burner rig tests. Instead, only samples Sm and Et showed significant peak shifts. These findings were compatible and in good agreement with results obtained by residual stress measurements (paragraph 3.5), and pointed out that modifications of S_{res} beard the prime responsibility of the observed changes of the (220) peak positions. Therefore, if analyzed in combination with average residual stress evaluations, X-ray spectra could confirm the improved Il stability and, in turn its high temperature oxidation resistance.

In this study, even if the film/substrate interface design endorsed a coating average residual stress modification, it did not induce any texture variation (for selected deposition conditions). In particular, the Ti-Al interlayer (α-type hexagonal microstructure; a=2.9775 Å and c=4.685 Å; crystallite size about 13 nm; estimated composition 60 at.% Al and 40 at. % Ti; slight (002) and (103) fiber texture) did not affect the just deposited sample Il texture. Generally, for

films with low residual stress and loose columnar structure, grains can align with the orientation of the interlayer ones easily. Instead, for specimens with compact microstructures and high residual stresses, grains do not align with the orientation of the interlayer [49]. This behavior was further confirmed in the present research work. Indeed, HiPIMS specimens were deposited with a highly compact structure, and the effect of the interlayer texture became insignificant in the texture development of the nitride film.

Moving on to mechanical characterization, coating Et high compressive S_{res} plus the incorporation of an elevated level of defects could have been effectively increased its hardness value. But, from a thermodynamic perspective, this high residual stress and flaw density led to a microstructure instability of the film at elevated temperatures too. Veprek [50] made clear that several superhard coatings lost their superhardness when they were heat treated up to a temperature higher than the deposition one because of the relaxation of the compressive stress and defects resulting from the energetic ion bombardment during production. Mitterer [51] and Mayrhofer [52] suggested that promoting high defect densities to improve hardness might cause a reduced thermal stability due to the lower thermal activation required to initiate recovery in these sort of structures. Accordingly, it became reasonable to affirm the low resistance to thermal oxidation of the sample Et was due to its greater defectiveness.

In summary, this research work allowed verifying the influence of pre-treatment of substrates before deposition on high temperature oxidation resistance. In particular, the coating/substrate design affected S_{res} and recovery Δ%: performing a bland plasma etching and depositing a metallic interlayer, it was possible to achieve *the optimum*. All the used characterization techniques provided useful information for understanding experimental results, but only average residual stress evaluation seemed to permit identifying the best sample since the first mild BR treatment.

5. CONCLUSIONS

This research work purpose was to verify the correlation between film/substrate interface engineering and high temperature behavior of Ti-Al-N coatings deposited via reactive HiPIMS on γ-TiAl alloys. Therefore, identical films (equal sputtering conditions) were deposited on three undistinguishable substrates, obtained from the same γ-TiAl billet. Coating/substrate interfaces were deliberately modified in an effort to affect thermal stability in oxidizing atmospheres.

Contrary to expectations, even after the harshest BR test, sample Il still formed a thin Ti-Al mixed oxide followed by a Ti-Al-N plus oxygen layer (total thickness < 100 nm) and not a typical double-layer structure (i.e. an Al-rich top-layer and a Ti-rich sub-layer below). Ergo, a metallic glue-layer clearly promoted adhesion together with the growing of fine equiassic cristallites at the early stages of film deposition (about 500 nm) giving rise to a considerably high temperature oxidation resistance.

Additionally, thermal stability could be related to average residual stress and to its changes due to burner rig treatments. Recovery effects caused a reduction of the overall stress state of the material, which was significantly different for the three samples: just coating Il S_{res} values remained nearly unchanged.

To conclude, it could be stated high temperature oxidation effects could be investigated by the measurement of average residual stresses: even after a bland cycling oxidation test, clear indications on the coatings high temperature behavior could be achieved.

FUNDING

This work was supported by The Italian National Research Council – Italian Ministry of Economic Development agreement “Ricerca di SistemaElettrico Nazionale” (DELIBERAZIONE AEEGS 4 NOVEMBRE 2016, 628/2016/RDS).

ACKNOWLEDGEMENT

X ray diffraction data were acquired thanks to the collaboration with Dr. Rosalba Gerbasi at CNR-ICMATE Padova. FIB residual stress experiments were performed at the interdepartmental laboratory of electron microscopy (LIME) of University of “Roma TRE”, Rome, Italy, with the assistance of Dr. Daniele De Felicis.

REFERENCES

[1] P. Janschek, Wrought TiAl blades, Materials Today: Proceedings 2S (2015) S92–S97

[2] A. Rahmel, W.J. Quadakkers, M. Schütze, Fundamentals of TiAl oxidation – A critical review, Materials and Corrosion 46 (1995) 271–285

[3] P. Kofstad, High temperature corrosion, Elsevier Applied Science, Essex UK (1988)

[4] M. Schütze, S. Friedle, Oxidation Behavior of Intermetallic Titanium Aluminide Alloys, MRS Proceedings 1516 (2012) 77-88

[5] F. Appel, J.D.H. Paul, M. Oehring (Eds.), Gamma titanium aluminide alloys: science and technology, Wiley-VCH (2011) 433–463

[6] R. Pflumm, S. Friedle, M. Schütze, Oxidation protection of γ-TiAl-based alloys – A review, Intermetallics 56 (2015) 1–14

[7] C. Leyens, R. Braun, M. Frohlich, and P. Eh. Hovsepian, Recent progress in the coating protection of gamma titanium-aluminides, JOM 58 (1) (2006) 17-21

[8] S. Jeon, C.J. Van Tyne, H. Lee, Degradation of TiAlN coating by the accelerated life test using pulsed laser ablation, Ceramics International, 40 (2014) 8677-8685

[9] V. Kouznetsov, K. Macák, J.M. Schneider, U. Helmersson, and I. Petrov, A novel pulsed magnetron sputter technique utilizing very high target power densities, Surface & Coatings Technology 122, Issues 2–3 (1999) 290-293

[10] A. Anders, Discharge physics of high power impulse magnetron sputtering, Surface and Coatings Technology 205 (2011) S171-S177

[11] M. Samuelsson, D. Lundin, J. Jensen, M. A. Raadu, J. T. Gudmundsson, U. Helmersson, On the film density using high power impulse magnetron sputtering, Surface & Coatings Technology, 205 (2010) 591-596

[12] M. Lattemann, A.P. Ehiasarian, J. Bohlmark, P.Å.O. Persson, U. Helmersson, Investigation of high power impulse magnetron sputtering pretreated interfaces for adhesion

enhancement of hard coatings on steel, Surface and Coatings Technology 200, 22–23 (2006) 6495–6499

[13] T. Shimizu, H. Komiya, T. Watanabe, Y. Teranishi, H. Nagasaka, K. Morikawa, M. Yanga, HiPIMS deposition of TiAlN films on inner wall of micro-dies and its applicability in micro-sheet metal forming, Surface & Coatings Technology250 (2014) 44–51

[14] M. Lattemann, U. Helmersson, J.E. Greene, Fully dense, non-faceted 111-textured high power impulse magnetron sputtering TiN films grown in the absence of substrate heating and bias, Thin Solid Films 518 (2010) 5978–5980

[15] C. Badini, S.M. Deambrosis, O. Ostrovskaya, V. Zin, E. Padovano, E. Miorin, M. Castellino, S.Biamino, Cyclic oxidation in burner rig of TiAlN coating deposited on Ti-48Al-2Cr-2Nb by reactive HiPIMS, Ceramics International 43 (2017) 5417-5426

[16] S. Biamino. A. Penna, U. Ackelid, S. Sabbadini, O. Tassa, P. Fino, M. Pavese, P. Gennaro, C. Badini, Electron beam melting of Ti-48Al-2Cr-2Nb alloy: microstructure and mechanical properties investigation, Intermetallics 19/6 (2011) 776-781

[17] A. P. Ehiasarian, J. G. Wen, I. Petrov, Interface microstructure engineering by high power impulse magnetron sputtering for the enhancement of adhesion. J. Appl. Phys. 101 (2007) 054301.

[18] K. D. Bakoglidis, S. Schmidt, G. Greczynski, L. Hultman, Improved adhesion of carbon nitride coatings on steel substrates using metal HiPIMS pretreatments, Surface & Coatings Technology 302 (2016) 454–462

[19] C. Badini, S.M. Deambrosis, E. Padovano, M. Fabrizio, O. Ostrovskaya, E. Miorin, G. D'Amico, F. Montagner, S. Biamino, V. Zin, Thermal Shock and Oxidation Behavior of HiPIMS TiAlN Coatings Grown on Ti-48Al-2Cr-2Nb Intermetallic Alloy, Materials 9, 12 (2016) 961.

[20] European Standard EN 1071-2, Advanced technical ceramic –Methods of test for ceramic coatings – Part 2: Determination of coating thickness by the crater grinding method

[21] J. M. Fildes, S. J. Meyers, R. Kilaparti, E. Schlepp, Improved Ball Crater Micro-Abrasion Test Based on a Ball on Three Disk Configuration. Wear 274–275 (2012) 414-422

[22] W. Rasband, Image J 1.51r version, National Institute of Health, USA. http://imagej.nih.gov/ij (accessed 18 April 2018)

[23] ISO 25178 - Geometrical product specifications (GPS) - Surface texture: Areal - Part 2: Terms, definitions and surface texture parameters, https://www.iso.org/obp/ui/#iso:std:iso:25178:-2:ed-1:v1:en

[24] ISO 4287 - Geometrical Product Specifications (GPS) - Surface texture: Profile method - Terms, definitions and surface texture parameters, https://www.iso.org/standard/10132.html

[25] S.M. Deambrosis, E. Miorin, F. Montagner, V. Zin, M. Fabrizio, M. Sebastiani, F. Massimi, E. Bemporad, Structural, morphological and mechanical characterization of Mo sputtered coatings, Surface & Coatings Technology 266 (2015) 14–21

[26] UNI EN 1071-3 European standard: Advanced technical ceramics - Methods of test for ceramic coatings - Determination of adhesion and other mechanical failure modes by a scratch test

[27] A. M. Korsunsky, M. Sebastiani, E. Bemporad, Residual stress evaluation at the micrometer scale: analysis of thin coatings by FIB milling and digital image correlation. Surface and Coatings Technology 205, Issue 7 (2010) 2393-2403

[28] M. Sebastiani, C. Eberl, E. Bemporad, G. M.Pharr, Depth-resolved residual stress analysis of thin coatings by a new FIB–DIC method, Materials Science and Engineering: A 528, Issue 27 (2011) 7901-8

[29] K. Kothari, R. Radhakrishnan, N.M. Werely, Advances in gamma titanum aluminides and their manufacturing technologies, Progress in Aerospace Sciences, 55 (2012) 1-16

[30] A. Bartels and W. Schillinger, Micromechanical Mechanism of Texture Formation in γ – TiAl, Intermetallics 9 (2001) 883–889

[31] A. Bartels, H. Kestler, and H. Clemens, Deformation Behavior of Differently Processed γ -Titanium Aluminides, Mater. Sci. Eng. A 329 (2002) 153–162

[32] S. Inamura, K. Nobugai, F. Kanamaru, The preparation of NaCl-type Ti1-xAlxN solid solution, Journal of Solid State Chemistry 68 (1987) 124-127

[33] T. Ikeda, H. Satoh, Phase formation and characterization of hard coatings in the TiAlN system prepared by the cathodic arc ion plating method, Thin Solid Films (1991) 195 99-110

[34] K. Kutschej, P.H. Mayrhofer, M. Kathrein, P. Polcik, R. Tessadri, C. Mitterer, Structure, mechanical and tribological properties of sputtered $Ti_{1-x}Al_xN$ coatings with $0.5 \leq x \leq 0.75$, Surface & Coatings Technology 200 (2005) 2358–2365

[35] C.V. Falub, A. Karimi, F. Fontaine and W. Kalss, Fiber texture dependence of the anisotropic residual stress state induced by lattice distortion in arc-evaporated Ti-Al-N thin films, Reviews on advanced materials science 15 (2007) 105-110

[36] J.P. Zhao, X. Wang, T.S. Shi, and X.H. Liu, Evolution of the texture of TiN films prepared by filtered arc deposition, Journal of Applied Physics 79 (1996) 9399

[37] J.T. Chen, J. Wang, F. Zhang, G.A. Zhang, X.Y. Fan, Z.G. Wu, P.X. Yan, Characterization and temperature controlling property of TiAlN coatings deposited by reactive magnetron co-sputtering, Journal of Alloys and Compounds 472 (2009) 91–96

[38] J. A. Thornton, The microstructure of sputter-deposited coatings, J. Vac. Sci. Technol. A 4 (1986) 3059-3065

[39] L.J. Gibson, M.F. Ashby, The mechanics of three-dimensional cellular materials, Proceedings of the Royal Society A 382 (1982) 43–59

[40] D. McIntyre, J.E. Greene, G. Hakansson, J.-E. Sundgren, W.-D. Münz, Oxidation of metastable single-phase polycrystalline Ti0.5Al0.5N films: Kinetics and mechanisms, J. Appl. Phys. 67 (3) (1990) 1542

[41] F. Vaz, L. Rebouta, M. Andritschky, M.F. da Silva, J.C. Soares, Thermal oxidation of Ti1-xAlxN coatings in air, J. Eur. Ceram. Soc. 17 (1997) 1971–1977

[42] T. Sprute, W. Tillmann, D. Grisales, U. Selvadurai, G. Fischer, Influence of substrate pre-treatments on residual stresses and tribo-mechanical properties of TiAlN-based PVD coatings, Surface & Coatings Technology 260 (2014) 369–379

[43] P. H. Mayrhofer, C. Mitterer, L. Hultman, H. Clemens, Microstructural design of hard coatings Progress in Materials Science 51 (2006) 1032–1114

[44] B.D. Cullity, Elements of X-Ray Diffraction 2nd ed., Addison-Wesley Publishing Company, Inc., 1978

[45] A. J. Perry, The state of residual stress in TiN films made by physical vapor deposition methods; the state of the art, Journal of Vacuum Science & Technology A: Vacuum, Surfaces, and Films 8 (1990) 1351-1358

[46] K. Ait Aissa, A. Achour, J. Camus, L. Le Brizoual, P. Y. Jouan, M. A. Djouadi, Comparison of the structural properties and residual stress of AlN films deposited by dc magnetron sputtering and high power impulse magnetron sputtering at different working pressures, Thin Solid Films 550 (2014) 264-267

[47] S. Grasser, R. Daniel, C. Mitterer, Microstructure modifications of CrN coatings by pulsed bias sputtering, Surface & Coatings Technology 206 (2012) 4666–4671

[48] R. Daniel, K.J. Martinschitz, J. Keckes, C. Mitterer, The origin of stresses in magnetron-sputtered thin films with zone T structures, Acta Materialia 58 (2010) 2621–2633

[49] Jia-HongHuang, Cheng-HsinMa, HaydnChen, Effect of Ti interlayer on the residual stress and texture development of TiN thin films deposited by unbalanced magnetron sputtering, Surface & Coatings Technology 201 (2006) 3199-3204

[50] S. Veprek, M. Jilek, Superhard nanocomposite coatings. From basic science toward industrialization, Pure Appl. Chem. 74 (3) (2002) 475

[51] C. Mitterer, P.H. Mayrhofer, J. Musil, Thermal stability of PVD hard coatings, Vacuum 71 (2003) 279-284

[52] P.H. Mayrhofer, C. Mitterer, High-temperature properties of nanocomposite TiBxNy and TiBxCy coatings, Surface & Coatings Technology 133 (2000) 131-137

LIST OF FIGURES CAPTIONS

Figure 1. A test performed on a Ti-Al-N coating deposited on a γ-TiAl based substrate. The residual stress in the central stub (~ 5 μm inner diameter) is progressively relaxed as the depth of the trench increases, thus giving measurable strains on the top surface. They are calculated from the SEM micrographs by a specifically developed DIC procedure. Microstructural features over the surface are sufficient to guarantee a very accurate displacement measurement.

Figure 2. γ-TiAl based substrate (Sub 1, 2, 3, 4) and Ti-Al-N coatings optical microscope (OP) and SEM images just after deposition, after 40 BR cycles up to 850 °C and 100 cycles up to 950 °C. Sm films were flat, compact and uniform; Et layers clearly reproduced the substrate solidification structure highlighted by the strong plasma etching; Il coating still allowed seeing the billet solidification structure. After the 850 °C test, no obvious differences between the three HiPIMS samples could be detected. After 100 cycles up to 950 °C, type Et films were discarded; Il coatings were morphologically quasi-intact.

Figure 3. XRD patterns collected from substrates in the as received state and after burner rig treatments (40 cycles up to 850 °C and 200 cycles up to 950 °C).

Figure 4. Normalized Ti-Al-N (220) peaks in XRD analyses performed on samples Sm, Et and Il.

Figure 5. (220) pole figure collected from sample Sm.

Figure 6. FIB images of the oxidized surfaces: the oxide scale was analyzed after each burner rig treatment. After 40 cycles up to 850 °C, it was not possible to measure Sm oxide film thickness: it was very thin and incoherent. Sample Et was not investigated up to 200 cycles at 950 °C: its behavior was comparable to bare TiAl one, already after 100 cycles up to 950 °C. In a) and c) the *small grain* layer is highlighted (white lines and arrows); in c) the Ti-Al metallic interlayer is shown too (red lines and arrows).

Figure 7. SEM micrographs of progressive loading scratch tests concerning samples Sm and Il, before and after 40 burner rig cycles at 850 °C. Failure points were highlighted by red circles.

Figure 8. Hardness (H) and elastic modulus (E) measured before and after burner rig thermal treatments (calculation depth 100 nm).

FIGURES

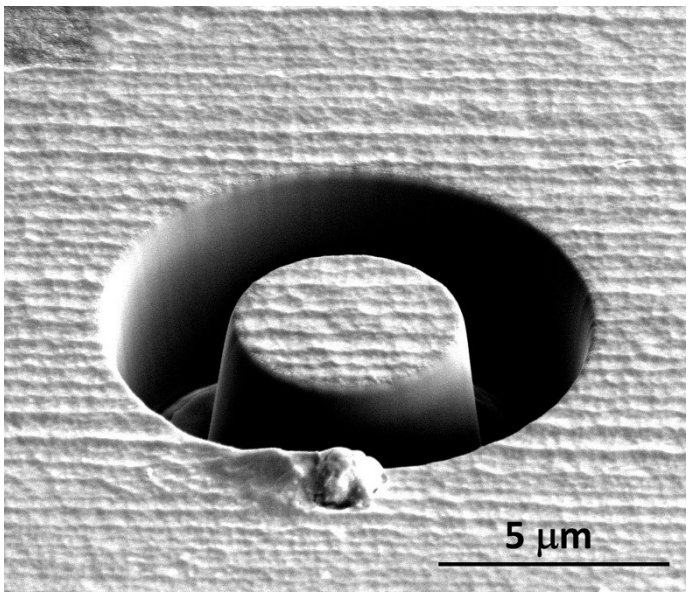

Figure 1

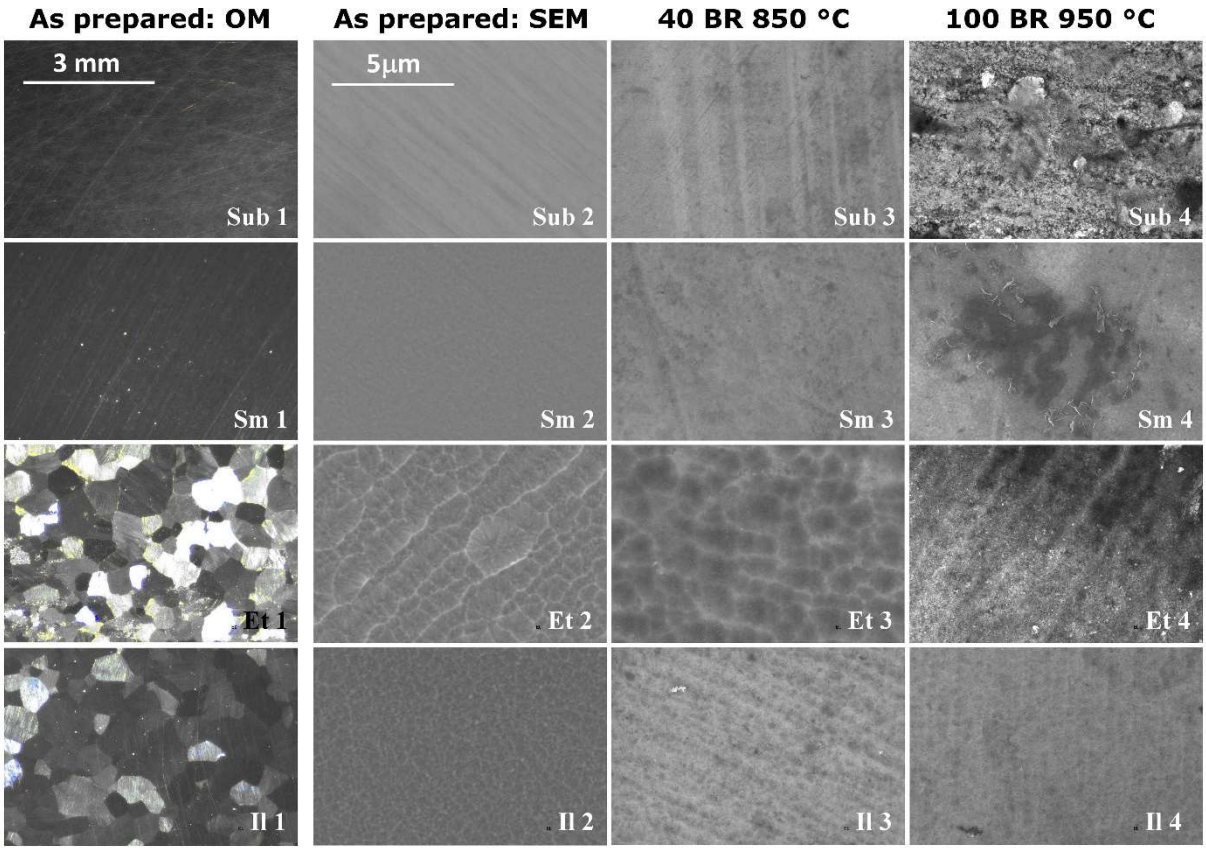

Figure 2

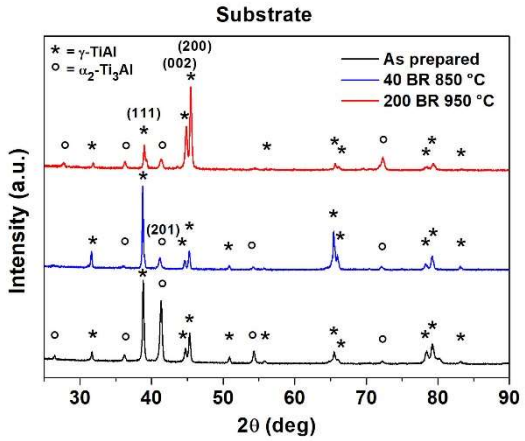
Substrate
* = γ-TiAl
o = α2-Ti3Al
(200)
(002)
(111)
(201)
As prepared
40 BR 850 °C
200 BR 950 °C
Intensity (a.u.)
30
40
50
60
70
80
90
2θ (deg)

Figure 3

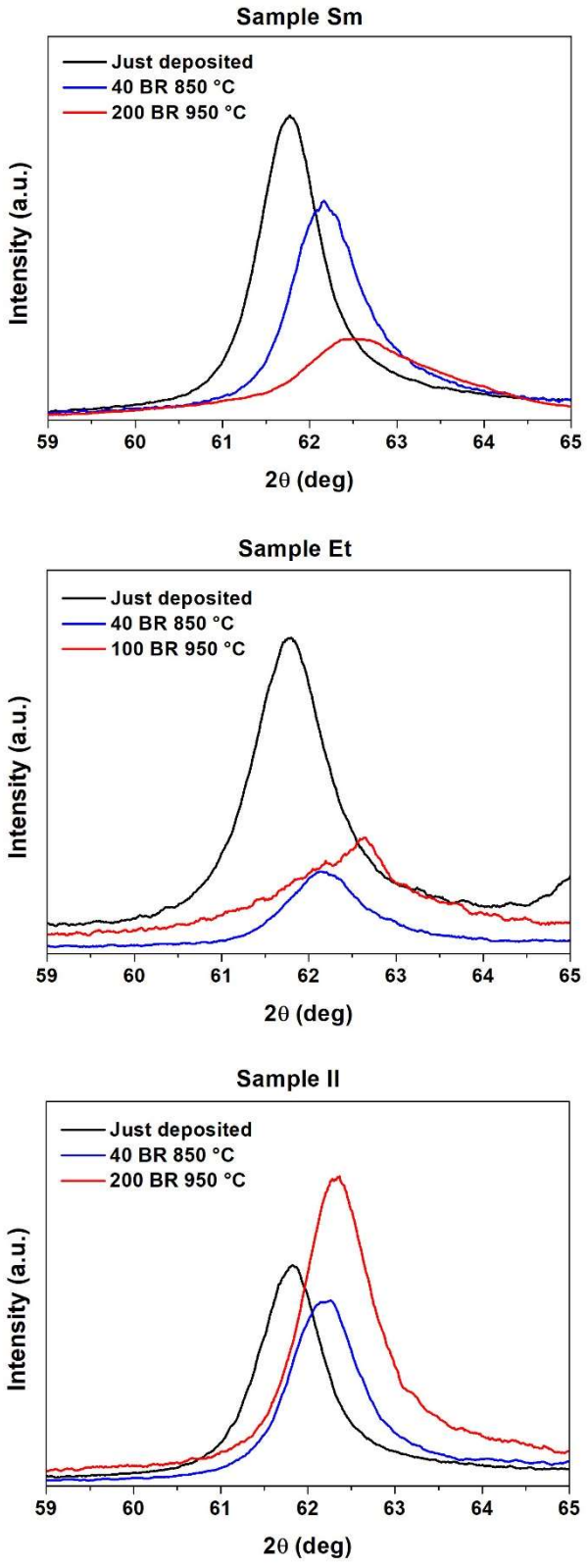
Sample Sm
Just deposited
40 BR 850 °C
200 BR 950 °C
Intensity (a.u.)
59
60
61
62
63
64
65
2θ (deg)
Sample Et
Just deposited
40 BR 850 °C
100 BR 950 °C
Intensity (a.u.)
59
60
61
62
63
64
65
2θ (deg)
Sample II
Just deposited
40 BR 850 °C
200 BR 950 °C
Intensity (a.u.)
59
60
61
62
63
64
65
2θ (deg)

Figure 4

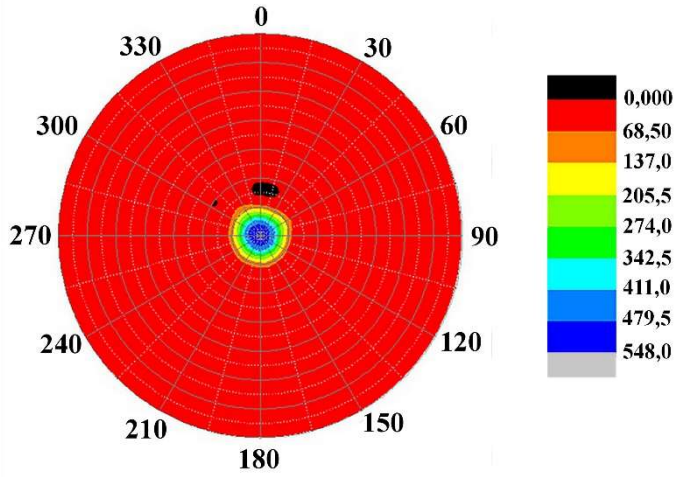

Figure 5

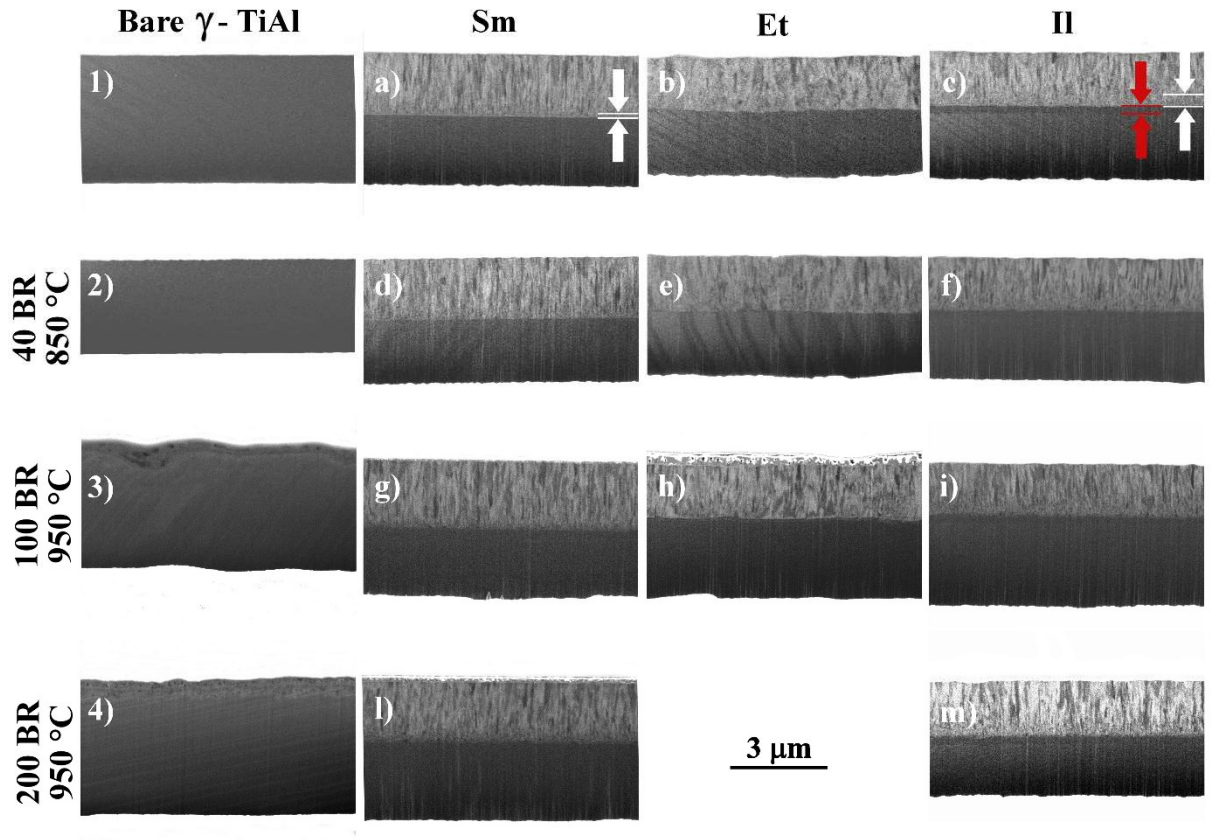

Figure 6

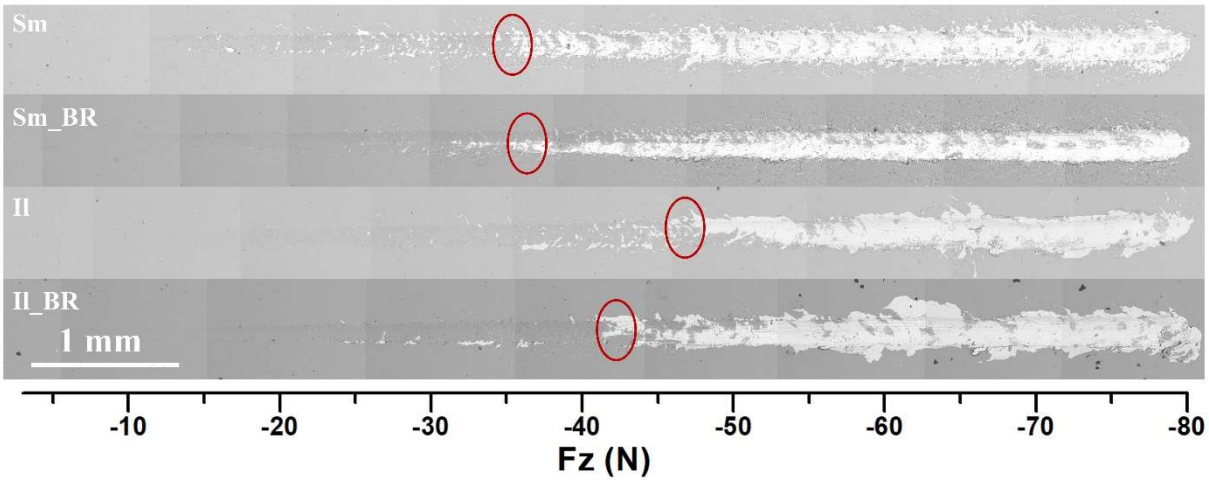

Figure 7

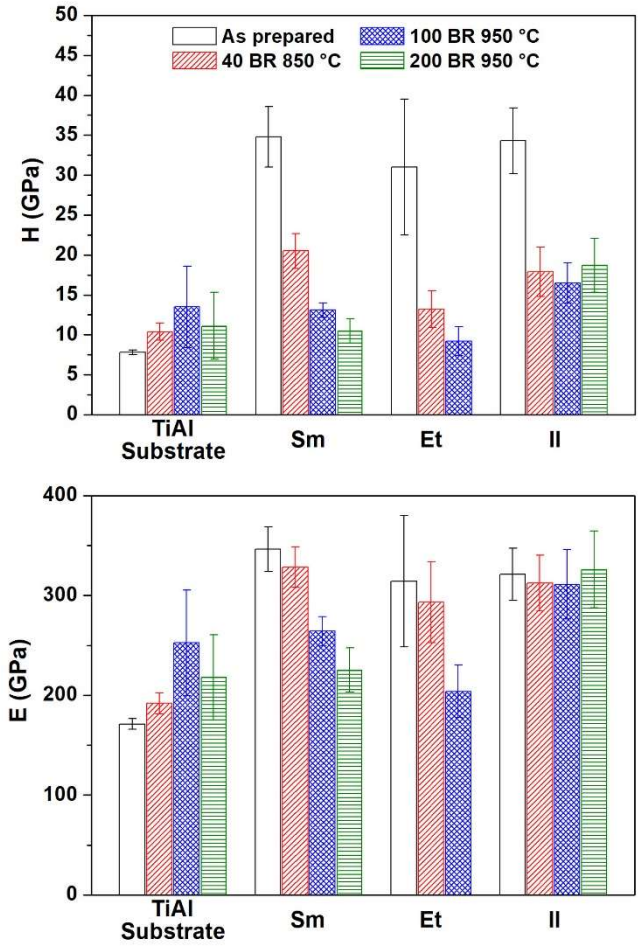

Figure 8